Pressure-driven superconducting dome in the vicinity of CDW in the pyrite-type superconductor CuS_2

L. F. Shi,[1,2] Z. Y. Liu,[1,3] J. Li,[1,2] X. X. Zhang,[1,2] N. N. Wang,[1,2] Q. Cui,[1,2] K. Y. Chen,[1,2] Q. Y. Liu,[3] P. T. Yang,[1,2] J. P. Sun,[1,2,*] B. S. Wang,[1,2] Y. Uwatoko,[4] Y. Sui,[3,5] H. X. Yang,[1,2] and J.-G. Cheng[1,2,†]

[1]*Beijing National Laboratory for Condensed Matter Physics and Institute of Physics, Chinese Academy of Sciences, Beijing 100190, China*

[2]*School of Physical Sciences, University of Chinese Academy of Sciences, Beijing 100190, China*

[3]*School of Physics, Harbin Institute of Technology, Harbin 150001, China*

[4]*Institute for Solid State Physics, University of Tokyo, Kashiwa, Chiba 277-8581, Japan*

[5]*Laboratory for Space Environment and Physical Sciences, Harbin Institute of Technology, Harbin 150001, China*

(Received 4 September 2021; accepted 23 December 2021; published 21 January 2022)

Prior to the superconducting transition at $T_c \approx 1.5$ K, the pyrite-type CuS_2 undergoes a charge-density-wave (CDW) transition at $T_s \approx 150$ K at ambient pressure. Here we studied the interplay between CDW and superconductivity (SC) in CuS_2 by tracking their evolutions with pressure via detailed measurements of resistivity and magnetic susceptibility under hydrostatic pressures up to 6.6 GPa. The high-quality CuS_2 samples used in the present study were synthesized under high-pressure and high-temperature conditions, and the formation of the $2\times2\times2$ supercell associated with the commensurate CDW order below T_s was confirmed by low-temperature transmission electron microscope. Our high-pressure results uncover a pressure-driven superconducting dome with an enhanced $T_c^{max} \sim 2.3$ K at $\sim$1.8 GPa accompanying the gradual suppression of the CDW order. This work thus demonstrates the competing nature between CDW and SC in the pyrite-type superconductor CuS_2.

DOI: 10.1103/PhysRevMaterials.6.014802

I. INTRODUCTION

Unveiling the relationship between superconductivity (SC) and other electronic orders has been an important topic in condensed-matter physics because it can provide important insights about the superconducting mechanism and useful guidelines for exploring new superconductors. For example, the occurrence of high-T_c SC on the border of long-range antiferromagnetic order in the cuprate [1] and iron-pnictide superconductors [2] highlights the essential role of critical spin fluctuations for mediating the cooper pairs, and thus it motivates extensive endeavors to explore novel unconventional superconductors in the vicinity of the magnetic quantum critical point (QCP) [3,4]. In addition to the spin degree of freedom, the interplay between charge density wave (CDW) and conventional SC, both involving strong electron-phonon coupling and Fermi surface instability, has also been actively studied, revealing the complex coexistence and/or competition relationships in response to external stimuli such as chemical doping [5] and applying pressure [6–8]. The enhancement of T_c in conjunction with the suppression of CDW order is frequently observed, e.g., in the layered transition-metal dichalcogenides (TMDs) $TiSe_2$ [9] and $Ta(Se, S)_2$ [10]. To gain more insights into the relationship between CDW and SC, here we focus on a pyrite-type superconductor CuS_2 with CDW order.

Among the $3d$ TMDs MX_2 (M = Mn, Fe, Co, Ni, Cu, Zn; X = S, Se, Te) compounds with the pyrite-type structure, CuX_2 are the only superconductors with T_c values of 1.5, 2.4, and 1.3 K for X = S, Se, and Te, respectively [11–13]. These CuX_2 pyrites can be stabilized by high-pressure and high-temperature (HPHT) synthesis. In contrast to $CuSe_2$ and $CuTe_2$ which exhibit a plain superconducting transition at low temperatures, CuS_2 was found to display another two transitions prior to the superconducting transition: it first undergoes a second-order phase transition at $T_s \approx 150$ K and then a first-order transition at $T_u \approx 50$ K [14–18].The former transition is manifested by pronounced anomalies in various physical properties, including a rapid decrease of magnetic susceptibility [18], a humplike anomaly in the metallic resistivity [18], and the linewidth broadening of the nuclear magnetic resonance (NMR) spectra [19]. The observation of superlattice spots in the electron diffraction pattern [20] below T_s has suggested the formation of CDW, which, however, seems to contradict with the Hall coefficient results that showed no obvious anomaly around T_s [17]. Thus, the nature of the transition at T_s has been the subject of a recent comprehensive theoretical investigation, which identified a previously unreported Kohn anomaly pertinent to the Fermi surface nesting vector and a $2\times2\times2$ periodic charge modulation associated with the motion of the S_2 dimers below $\sim$100 K driven by a slight orbital occupation imbalance of the copper d and sulfur p orbitals [21]. These results support the occurrence of CDW order in CuS_2 and make it a previously unrealized candidate to study the interplay between SC and CDW. The low-temperature transition at T_u

*jpsun@iphy.ac.cn
†jgcheng@iphy.ac.cn

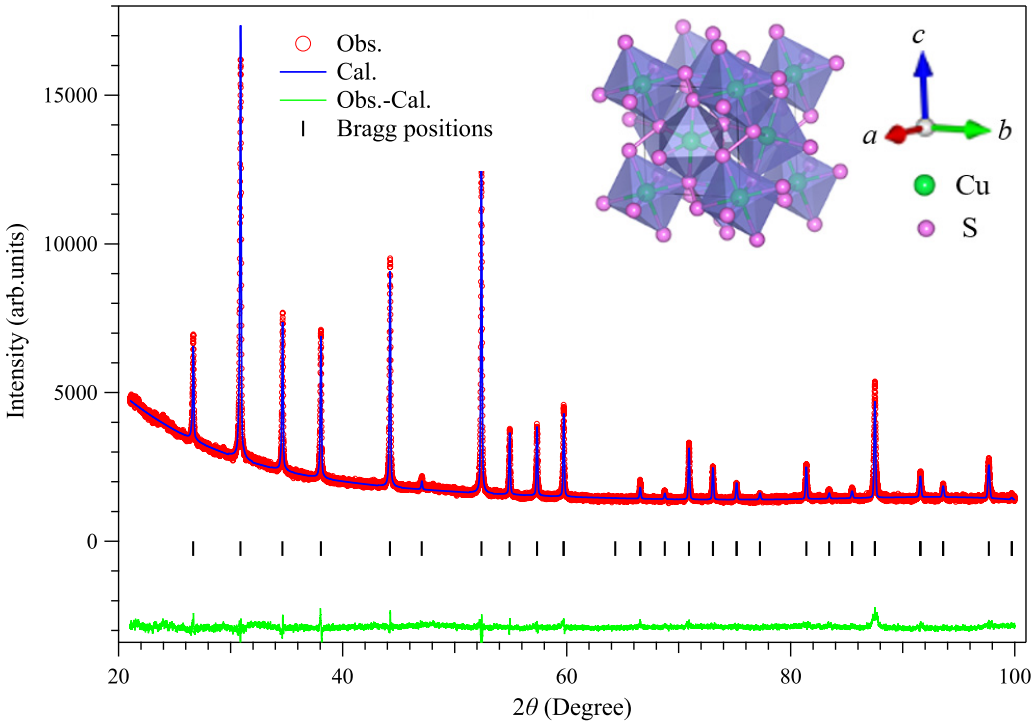

FIG. 1. Observed (open circle), calculated (solid line), and difference (bottom line) XRD profiles of the CuS_2 powder sample after Rietveld refinement. The Bragg positions are shown by vertical marks. The inset shows the crystal structure of CuS_2.

has been characterized by a sharp peak in the magnetic susceptibility and a weak sudden change of lattice parameter. Strangely, no obvious anomaly can be discerned in other physical properties such as resistivity and specific heat around $T_u \approx 50$ K [18]. The origin of the latter transition remains unclear so far. Following these previous studies on CuS_2, the purpose of this work is to study the interplay between CDW and SC.

In this work, we synthesized pure CuS_2 bulk samples under HPHT conditions and characterized its physical properties at ambient pressure. Importantly, we determined directly the $2\times2\times2$ superstructure using a low-temperature transmission electron microscope (TEM), confirming the occurrence of commensurate CDW order below T_s. Then, we studied the interplay between CDW and SC by monitoring the evolution of their transition temperatures as a function of pressure via detailed measurements of electrical resistivity and magnetic susceptibility under various hydrostatic pressures. Our results uncover a pressure-driven superconducting dome with enhanced T_c associated with the concomitant suppression of the CDW transition, thus demonstrating the competing nature between these two electronic orders in CuS_2.

II. EXPERIMENTAL DETAILS

Polycrystalline CuS_2 samples used in the present study were prepared by sintering a stoichiometric mixture of CuS and S powders at 5 GPa and 900 °C for 1 h with a Kawai-type multianvil module (Max Voggenreiter GmbH). Several pellets of the mixture were contained in a cylindrical h-BN crucible, which was inserted in a graphite sleeve that served as a heater, and pyrophyllite plugs were stuffed at both ends of the heater. The sample assembly was put in the central hole of an octahedral pressure medium made of 580-OF. During the HPHT experiments, the sample was first compressed to the desired pressure by eight truncated tungsten carbide cubes with TEL = 8 mm. Then, the temperature was increased to 900 °C and kept for 1 h before quenching to room temperature. The sample recovered after releasing pressure was characterized at ambient pressure.

Phase purity of the obtained samples was examined by powder x-ray diffraction (XRD) at room temperature (Cu $K\alpha$ radiation, $\lambda = 1.5408$ Å). Structural parameters were extracted from the XRD pattern via Rietveld refinement with the FULLPROF program. *In situ* low-temperature TEM was performed using a liquid-helium-cooled specimen holder (GATAN, HCHDT3010) in a JEM-2100F electron microscope equipped with a charge-coupled-device camera system and operated at 200 keV. The specimens for TEM observation were prepared by mechanical crushing, i.e., cleaved pieces were crushed in an agate mortar and deposited directly onto a holey carbon copper grid with the aid of ethanol.

Direct current (dc) magnetic susceptibility and isothermal magnetization at different temperatures down to 0.4 K were measured with a commercial Magnetic Property Measurement System (MPMS-III, Quantum Design) equipped with a ^{3}He insert (iHelium3). Measurements of resistivity with a standard four-probe configuration at ambient pressure were carried out by using the Physical Property Measurement System (PPMS, Quantum Design) from 300 to 2 K.

High-pressure resistivity measurements with a standard four-probe configuration were performed under hydrostatic

pressures up to 2.2 GPa with a self-clamped piston-cylinder cell (PCC) and up to 6.6 GPa with a palm-type cubic anvil cell (CAC), respectively. We also measured ac magnetic susceptibility by the mutual inductance technique using a PCC. The sample and a piece of lead (Pb) with similar volume were put into the coil and fixed by glue. The superconducting shielding volume fraction of the sample was estimated by comparing its diamagnetic signal with that of Pb. The pressure values in PCC were determined from the superconducting transition of Pb according to the following equation: $P(\mathrm{GPa}) = (T_0 - T_c)/0.365$, where $T_0 = 7.20$ K is the T_c of Pb at ambient pressure. The pressure in CAC was estimated from the calibration curve at low temperatures. For these high-pressure measurements, liquid pressure-transmitting media, i.e., Daphne 7373 for PCC and glycerol for CAC, were used to ensure excellent hydrostatic pressure conditions.

III. RESULTS AND DISCUSSION

The resultant pellet after HPHT synthesis is dark purple with metallic luster. Figure 1 shows the powder XRD pattern after Rietveld refinements for the CuS_2 sample at room temperature. It confirms that the as-obtained sample is single-phase with a pyrite-type structure in the cubic space group $Pa\bar{3}$ (no. 205). The refinement converged well with reliability factors $R_p = 2.75\%$, $R_{wp} = 3.59\%$, and $\chi^2 = 2.61$. The obtained lattice parameter $a = 5.7873(7)$ Å is in good agreement with that reported previously [13]. The crystal structure of CuS_2 is illustrated in the inset of Fig. 1. Each Cu atom is surrounded by six S atoms to form a compressed octahedron along the trigonal axis. These CuS_6 octahedra located at the face-centered-cubic (fcc) positions are connected through the S_2 units, the center of which are on the alternate points of a NaCl-type lattice. Each S atom is coordinated by three Cu atoms and another S atom (the other half of the S_2 unit) at the corners of a tetrahedron. Alternatively, the pyrite structure of CuS_2 can be viewed as an interpenetrating fcc array of Cu atoms and S_2 dimers as in the rocksalt structure.

Temperature dependences of resistivity $\rho(T)$ and magnetic susceptibility $\chi(T)$ shown in Fig. 2 confirm the presence of three characteristic phase transitions in CuS_2 at ambient pressure. All these results are consistent with those reported previously [17,18]. As displayed in Fig. 2(a), the $\rho(T)$ shows a metallic behavior in the whole temperature range with residue resistivity ratio $\mathrm{RRR} = \rho(300\ \mathrm{K})/\rho(2\ \mathrm{K}) \sim 28$, and it exhibits a humplike anomaly at $T_s = 145$ K, which can be determined from the minimum of $d\rho/dT$. As mentioned above, this anomaly is due to the formation of CDW order [20]. Upon further cooling down, CuS_2 is confirmed to enter the superconducting state with a sharp superconducting transition $\Delta T_c = 0.005$ K below $T_c^{\mathrm{onset}} = 1.57$ K, as shown in the upper inset of Fig. 2(a). The observed sharp superconducting transition and high RRR further elaborate the high quality of the obtained sample. The $\chi(T)$ curves shown in Fig. 2(b) were recorded under an external magnetic field of 1 T in both zero-field-cooled (ZFC) and field-cooled (FC) modes. As can be seen, the $\chi(T)$ curves first experience a rapid decrease at T_s and then display an abrupt spikelike anomaly at $T_u \approx 50$ K;

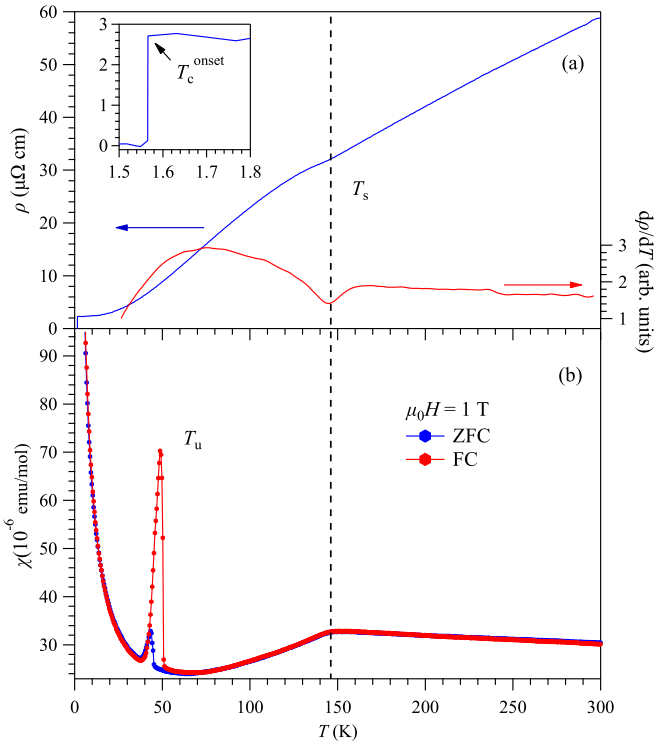

FIG. 2. Temperature dependences of (a) resistivity $\rho(T)$ at zero field and (b) magnetic susceptibility $\chi(T)$ under $\mu_0 H = 1$ T for the CuS_2 sample in both zero-field-cooled (ZFC) and field-cooled (FC) modes. The upper left inset of (a) shows the enlarged view of the superconducting transition at low temperatures. The anomalies in $\rho(T)$ and $\chi(T)$ are marked by the dashed line.

the magnitude of the spike in the FC curve is much stronger than that in the ZFC curve. Similar to the previous report [18], there is no discernable anomaly in $\rho(T)$ around T_u, Fig. 2(a). We also carefully checked the specific heat and found no anomaly around T_u as shown in Fig. S1 of the supplemental material [22]. It is thus very intriguing why such a pronounced anomaly in $\chi(T)$ shows no indication in the electrical and thermodynamic properties. The strong tail of $\chi(T)$ at low temperature should be attributed to the paramagnetic impurities.

The occurrence of the CDW transition at T_s in CuS_2 is further elaborated by the low-temperature TEM measurements. Figure 3 shows the typical selected area electron diffraction (SAED) patterns taken along the $[1\bar{1}0]$ zone axes at 294 and 25 K, respectively. As shown in Fig. 3(b), the weak superlattice spots $\frac{1}{2}\langle 2m+1,\ 2n+1,\ 2p+1\rangle$ (with m, n, p integers) appear at low temperatures, indicating the formation of the $2\times2\times2$ supercell, which is consistent with the recent theoretical prediction [21]. Similar CDW related diffraction spots can also be observed in other CDW systems, such as $NbSe_2$ and $TaSe_2$ [23]. No extra spots can be observed along $[1\bar{1}0]$ and other low-index zone axes (see Fig. S2 of the Supplemental Material [22]), once again proving the high-phase purity of the synthesized samples.

Before studying the interplay between CDW and SC, we first characterized in detail the superconducting properties of CuS_2 at ambient pressure. Figure 4(a) shows the dc

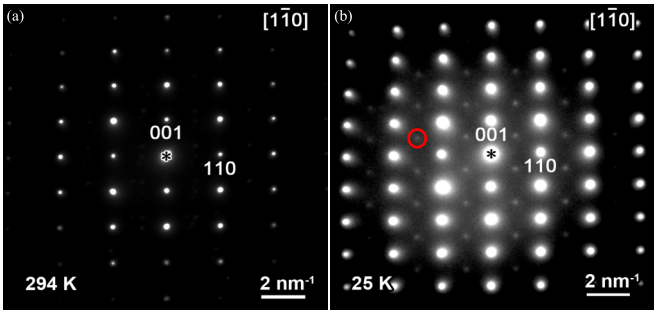

FIG. 3. Electron diffraction patterns showing the superlattice in CuS_2. Typical selected area electron diffraction (SAED) patterns taken along the [1$\bar{1}$0] zone axis at (a) 294 K and (b) 25 K, respectively. The 2×2×2 superlattice spots can be observed at low temperatures, as indicated by the red circle.

magnetic susceptibility $4\pi\chi_V(T)$ below 1.8 K measured at 5 Oe under both ZFC and FC processes. Bulk SC with a sharp superconducting transition at $T_c^{\chi} = 1.55$ K can be clearly seen from the sharp drop of $\chi(T)$, in perfect agreement with the zero-resistivity $\rho(T)$ data shown in Fig. 2(a). The low-field magnetic isotherms $M(H)$ from 0.4 to 1.4 K for CuS_2 are plotted in Fig. 4(b), which shows the common magnetic hysteresis loops of type-II superconductors. The lower critical field, $\mu_0 H_{c1}$, defined as the field where the $M(H)$ curve deviates from the linear behavior, decreases monotonically with increasing temperature, as shown in Fig. 4(c). Fitting to $\mu_0 H_{c1}(T)$ with the empirical Ginzburg-Landau (GL) equation, i.e., $\mu_0 H_{c1}(T) = \mu_0 H_{c1}(0)(1-t^2)/(1+t^2)$, where $t = T/T_c$, yields a zero-temperature $H_{c1}(0) = 123.2$ Oe. The upper critical field $\mu_0 H_{c2}$ is defined as the point where $M(H)$ reaches zero. As seen in Fig. 4(c), the $\mu_0 H_{c2}(T)$ can also be well described with the GL equation, giving rise to a zero-temperature $H_{c2}(0) = 502.9$ Oe. The obtained value is much larger than that of 160 Oe reported previously based on the specific-heat measurements [18]. The obtained $\mu_0 H_{c2}(0)$ can be used to estimate the GL coherence length $\xi_{GL} = 809$ Å based on the relationship $\mu_0 H_{c2}(0) = \Phi_0/2\pi\xi_{GL}^2$, where $\Phi_0 = hc/2e = 2.067\times10^{-7}$ Oe cm^2 is the magnetic flux quantum. Consequently, the calculated penetration depth is $\lambda_{GL}(0) = 901$ Å [24,25]. The GL parameter $\kappa_{GL} = \lambda_{GL}/\xi_{GL} = 1.11$ that is larger than $1/\sqrt{2}$ further confirms that CuS_2 belongs to the type-II superconductor.

To study the interplay between CDW and SC, we first measure the temperature dependences of resistivity $\rho(T)$ from 300 K down to 1.5 K under various pressures up to 2.2 GPa with a PCC. The data in the whole temperature range are displayed in Fig. 5(a), from which we can see the gradual suppression of the CDW transition with increasing pressure. To illustrate the evolution of CDW clearly, we plot in Fig. 5(c) the $\rho(T)$ and its derivative $d\rho/dT$ in the temperature range 50–200 K for $P \leqslant 1.6$ GPa. As can be seen, the humplike anomaly is gradually smeared out with increasing pressure to 1.6 GPa, and the T_s defined from the minimum of $d\rho/dT$ is shifted from

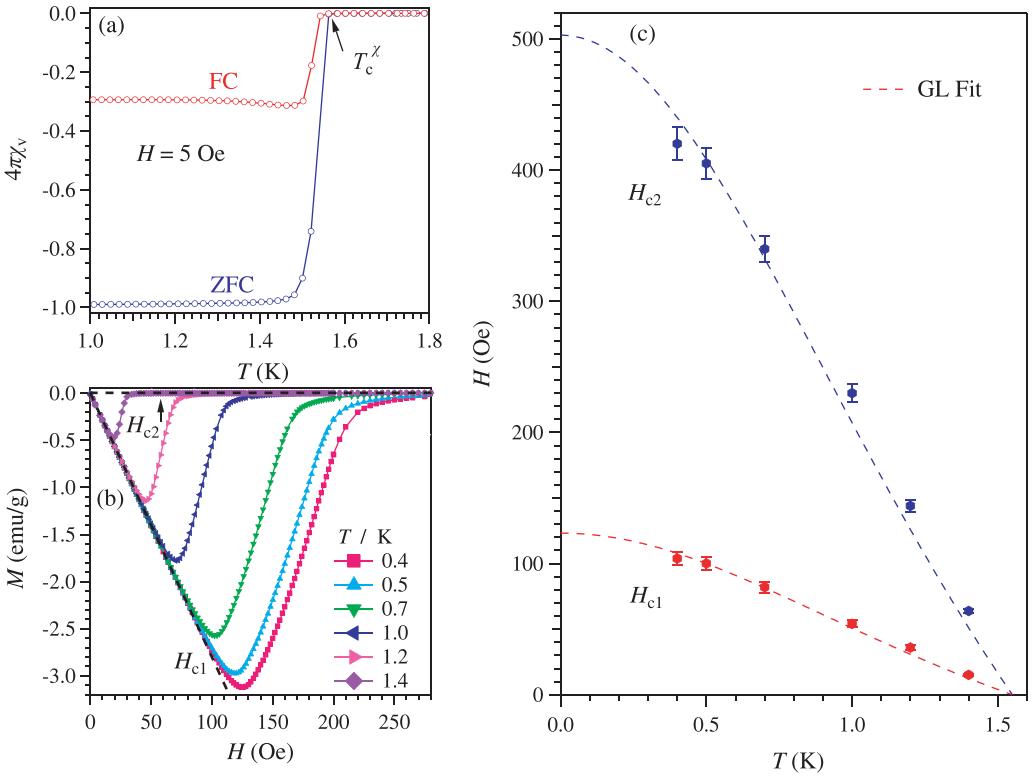

FIG. 4. (a) Temperature dependence of the magnetic susceptibility of CuS_2 measured in the ZFC and FC modes under an applied magnetic field of $\mu_0 H = 5$ Oe in the temperature range 1–1.8 K. (b) The isothermal magnetization $M(H)$ curves at different temperatures below T_c. (c) Temperature dependences of the lower critical field $\mu_0 H_{c1}$ and the upper critical field $\mu_0 H_{c2}$ of CuS_2 fitted by the Ginzburg-Landau (GL) formula.

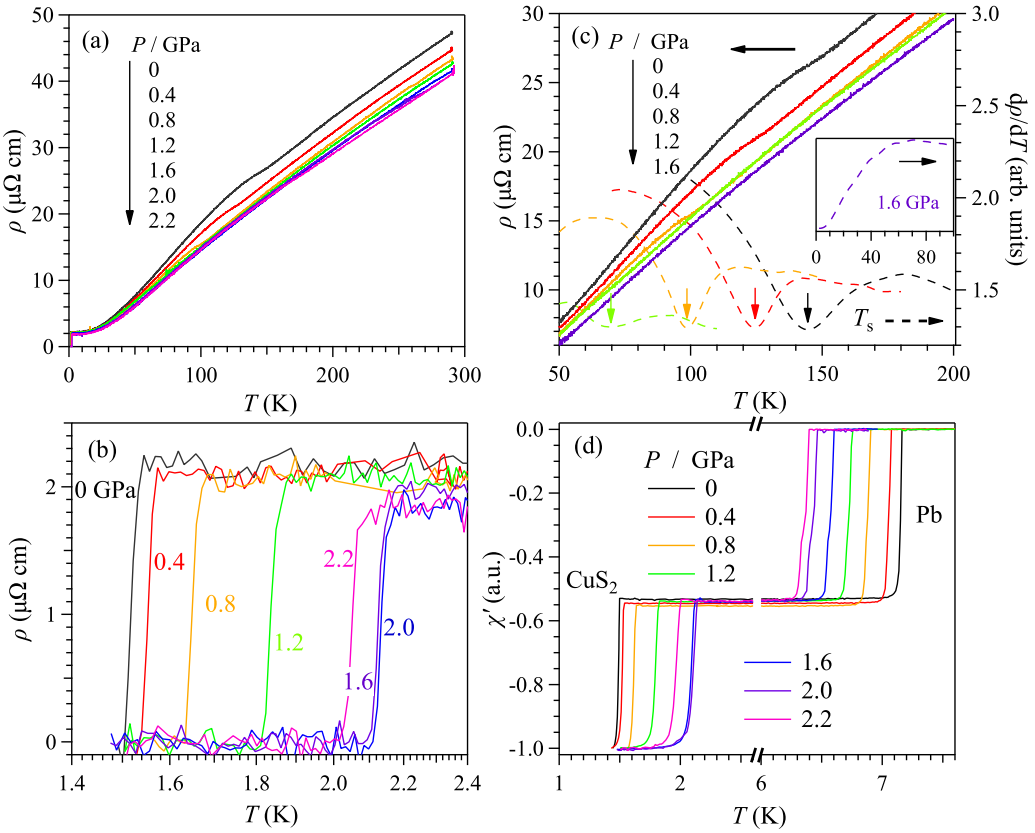

FIG. 5. (a) Temperature dependence of resistivity $\rho(T)$ between 300 and 1.4 K for CuS_2 under various pressures up to 2.2 GPa measured with a piston-cylinder cell (PCC). (b) An enlarged view of the superconducting transitions at low temperatures. (c) Temperature dependence of resistivity $\rho(T)$ (left axis) and its temperature derivative $d\rho/dT$ (right axis) at 0, 0.4, 0.8, 1.2, and 1.6 GPa, highlighting the evolution of the CDW transition T_s. (d) Temperature dependence of the ac magnetic susceptibility $\chi'(T)$ measured under various pressures. The pressure values shown in the figure are determined from the superconducting transition temperature of Pb shown in (d).

145 K at ambient pressure to ∼70 K at 1.2 GPa. The CDW transition cannot be discerned anymore above 1.2 GPa, which indicates that the long-range CDW order has been disrupted. It has been reported that substitution of Se for S in the series of $CuS_{2-x}Se_x$ can also suppress T_s [26], for which the chemical disorders rather than the negative chemical pressure should play the dominant role in suppressing the CDW order.

The evolution of the superconducting transition as a function of pressure is studied by the resistivity $\rho(T)$ and ac susceptibility $\chi'(T)$ measurements. An enlarged view of the low-temperature $\rho(T)$ data in Fig. 5(b) clearly shows that T_c first increases quickly from ∼1.5 K at 0 GPa to ∼2.1 K at 1.6–2 GPa and then decreases to ∼2 K at 2.2 GPa. The $\chi'(T)$ data shown in Fig. 5(d) further confirm the above resistivity results and verify the bulk character of the SC in the whole investigated pressure range. To further track the variation of T_c at higher pressures, we turn to the resistivity $\rho(T)$ measurements in CAC up to 6.6 GPa. The $\rho(T)$ data in Fig. 6(a) display no obvious anomaly in the whole temperature range except for the superconducting transition. Moreover, the $d\rho/dT$ data at 1.8 GPa in the inset of Fig. 6(a) show no indication of CDW order. As shown in Fig. 6(b), the T_c at the first pressure 1.8 GPa in CAC has reached ∼2.3 K, which is consistent with the PCC results at the similar pressures 1.6 and 2.0 GPa. As seen in Fig. 6(b), T_c of CuS_2 decreases monotonically upon further increasing pressure in CAC and reaches about 1.4 K at 3 GPa. No reentrant SC was observed at higher pressures up to 6.6 GPa.

The superconducting transition of CuS_2 in CAC is further characterized by measuring the field dependence of resistivity at 1.8 and 2.3 GPa. The data at 1.8 GPa are shown in Fig. 6(c), and those at 2.3 GPa are shown in Fig. S3 of the supplemental material [22]. As expected, the superconducting transition continuously shifts to the lower temperatures with increasing magnetic field. The temperature dependence of the upper critical field $\mu_0 H_{c2}(T)$ at 1.8 and 2.3 GPa is plotted in Fig. 6(d). GL fitting to these data yields $H_{c2}(0) = 584.8$ and 455.9 Oe for 1.8 and 2.3 GPa, respectively.

Based on the above high-pressure characterizations, we construct the temperature-pressure phase diagram of CuS_2, Fig. 7, which clearly depicts the relationship between CDW and SC as a function of pressure. As can be seen, $T_s(P)$ decreases monotonically with increasing pressure and cannot be discerned above 1.2 GPa, while $T_c(P)$ features a broad dome with the maxima around 1.8 GPa, which seems to be located at the putative critical point of $T_s(P)$. This observation implies a competitive relationship between CDW and SC in CuS_2. However, some features are noteworthy with regard to the special characters of CuS_2 as discussed below.

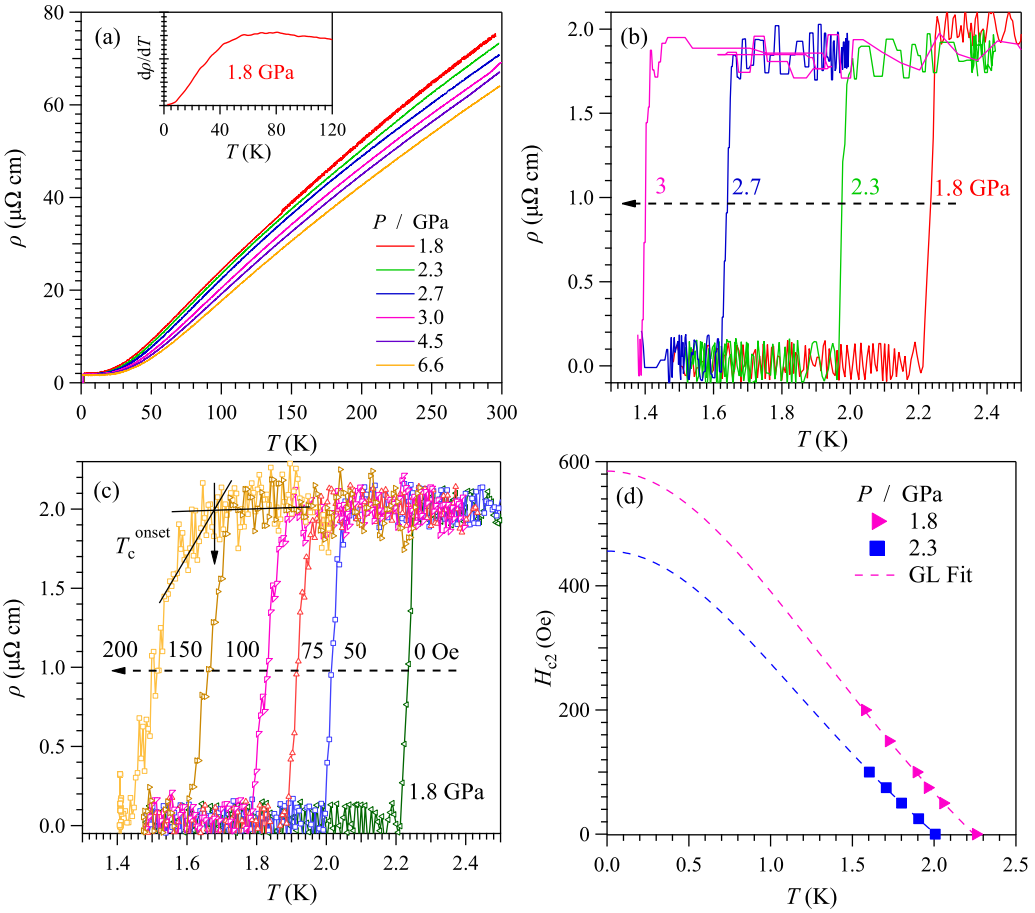

FIG. 6. (a) Temperature dependence of resistivity $\rho(T)$ between 300 and 1.4 K under various pressure up to 6.6 GPa measured in the cubic anvil cell (CAC). The inset of (a) shows $d\rho/dT$ data at 1.8 GPa. (b) An enlarged view of the superconducting transitions at low temperatures. (c) Temperature dependence of resistivity $\rho(T)$ at 1.8 GPa under various magnetic fields. (d) Upper critical field H_{c2} vs temperature at 1.8 and 2.3 GPa.

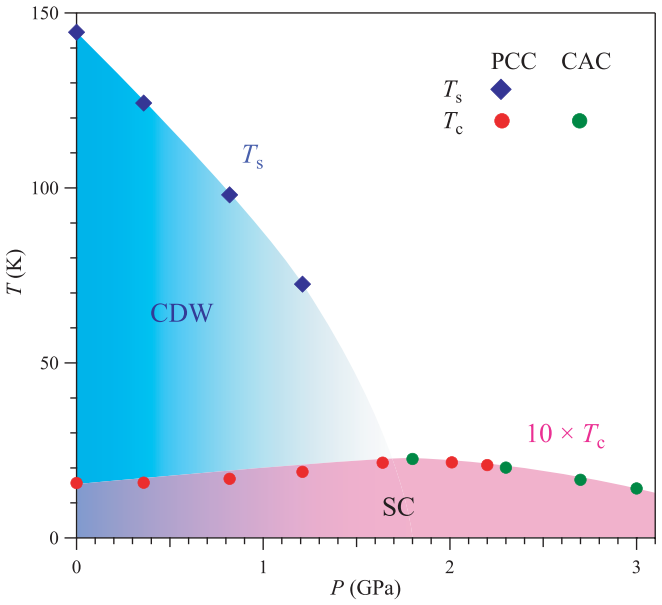

FIG. 7. Temperature-pressure phase diagram of CuS_2. The CDW temperature (T_{CDW}, blue filled square), and the superconducting transition temperature (T_c, red and green filled circles), were determined from the above high-pressure measurements in the PCC and CAC.

The coexistence of SC and CDW in CuS_2 at ambient pressure indicates that they arise from different portions of Fermi surfaces. With increasing pressure, CDW is gradually suppressed, and T_c is slightly enhanced, which should be attributed to the enhancement of electron density participating in the superconductivity under pressure. When CDW is completely suppressed, T_c shows a maximum and then begins to decrease with pressure. The possible origin is presumably due to the density of states at the Fermi level no longer increasing, and the phonon hardening under higher pressures.

However, in comparison with other TMDs with the CDW instabilities, such as Ta(Se, S)$_2$ [7,27,28], the observed enhancement of T_c in CuS_2 from 1.55 K at ambient pressure to the maximum of 2.3 K around 1.8 GPa is not significant. For these TMDs with the coexistence of SC and CDW, the enhancement of T_c under pressure should be mainly attributed to the suppression of CDW, which can increase the density of states at Fermi level available for cooper pairing as mentioned above. For most TMDs, the dominant contributions at the Fermi level come from the d electrons of transition metals, as seen in NbS_2 [29], TaS_2 [30], and Mo(S, Se, Te)$_2$ [31]. By contrast, previous studies on CuS_2 have shown that the p-states of sulfur contribute predominantly at the Fermi level [14,32]. This is probably the main reason why the

enhancement of T_c in CuS_2 is not significant when CDW is completely suppressed under pressure.

IV. CONCLUSION

In summary, we have synthesized the pyrite-type CuS_2 under 5 GPa and 900 °C and characterized its structural, transport, and magnetic properties at ambient pressure. We identified the $2\times2\times2$ superlattice at low temperatures by TEM. Then, we performed a comprehensive high-pressure study on the electrical transport and magnetic properties of the CuS_2. Our results reveal a pressure-induced suppression of the CDW order, and they uncover a superconducting dome with slightly enhanced T_c in the vicinity of CDW order, thus demonstrating the competing character between CDW and SC in CuS_2.

ACKNOWLEDGMENTS

This work is supported by the Beijing Natural Science Foundation (Z190008), National Natural Science Foundation of China (12025408, 11921004, 11888101, 11834016, 11904391, 12174424, and 11874400), the National Key R&D Program of China (2018YFA0305700 and 2018YFA0305800), the Strategic Priority Research Program and Key Research Program of Frontier Sciences of the Chinese Academy of Sciences (XDB25000000, XDB33000000, and QYZDB-SSW-SLH013), and the CAS interdisciplinary Innovation Team (JCTD-2019-01) as well as the Users with Excellence Program of Hefei Science Center CAS (Grant No. 2021HSC-UE008). Y.U. acknowledges the support from JSPS KAKENHI (JP19H00648).

[1] B. Keimer, S. A. Kivelson, M. R. Norman, S. Uchida, and J. Zaanen, From quantum matter to high-temperature superconductivity in copper oxides, Nature (London) **518**, 179 (2015).

[2] J. P. Sun, K. Matsuura, G. Z. Ye, Y. Mizukami, M. Shimozawa, K. Matsubayashi, M. Yamashita, T. Watashige, S. Kasahara, Y. Matsuda, J. Q. Yan, B. C. Sales, Y. Uwatoko, J. G. Cheng, and T. Shibauchi, Dome-shaped magnetic order competing with high-temperature superconductivity at high pressures in FeSe, Nat. Commun. **7**, 12146 (2016).

[3] W. Wu, J. Cheng, K. Matsubayashi, P. Kong, F. Lin, C. Jin, N. Wang, Y. Uwatoko, and J. Luo, Superconductivity in the vicinity of antiferromagnetic order in CrAs, Nat. Commun. **5**, 5508 (2014).

[4] J. G. Cheng, K. Matsubayashi, W. Wu, J. P. Sun, F. K. Lin, J. L. Luo, and Y. Uwatoko, Pressure Induced Superconductivity on the Border of Magnetic Order in MnP, Phys. Rev. Lett. **114**, 117001 (2015).

[5] Y. Liu, R. Ang, W. J. Lu, W. H. Song, L. J. Li, and Y. P. Sun, Superconductivity induced by Se-doping in layered charge-density-wave system $1T$-$TaS_{2-x}Se_x$, Appl. Phys. Lett. **102**, 192602 (2013).

[6] K. Y. Chen, N. N. Wang, Q. W. Yin, Y. H. Gu, K. Jiang, Z. J. Tu, C. S. Gong, Y. Uwatoko, J. P. Sun, H. C. Lei, J. P. Hu, and J. G. Cheng, Double Superconducting Dome and Triple Enhancement of T_c in the Kagome Superconductor CsV_3Sb_5 Under High Pressure, Phys. Rev. Lett. **126**, 247001 (2021).

[7] S. X. Xu, J. J. Gao, Z. Y. Liu, K. Y. Chen, P. T. Yang, S. J. Tian, C. S. Gong, J. P. Sun, M. Q. Xue, J. Gouchi, X. Luo, Y. P. Sun, Y. Uwatoko, H. C. Lei, B. S. Wang, and J. G. Cheng, Effects of disorder and hydrostatic pressure on charge density wave and superconductivity in $2H$-TaS_2, Phys. Rev. B **103**, 224509 (2021).

[8] N. N. Wang, K. Y. Chen, Q. W. Yin, Y. N. N. Ma, B. Y. Pan, X. Yang, X. Y. Ji, S. L. Wu, P. F. Shan, S. X. Xu, Z. J. Tu, C. S. Gong, G. T. Liu, G. Li, Y. Uwatoko, X. L. Dong, H. C. Lei, J. P. Sun, and J. G. Cheng, Competition between charge-density-wave and superconductivity in the kagome metal RbV_3Sb_5, Phys. Rev. Res. **3**, 043018 (2021).

[9] A. F. Kusmartseva, B. Sipos, H. Berger, L. Forró, and E. Tutiš, Pressure Induced Superconductivity in Pristine $1T$-$TiSe_2$, Phys. Rev. Lett. **103**, 236401 (2009).

[10] D. C. Freitas, P. Rodière, M. R. Osorio, E. Navarro-Moratalla, N. M. Nemes, V. G. Tissen, L. Cario, E. Coronado, M. García-Hernández, S. Vieira, M. Núñez-Regueiro, and H. Suderow, Strong enhancement of superconductivity at high pressures within the charge-density-wave states of $2H$-TaS_2 and $2H$-$TaSe_2$, Phys. Rev. B **93**, 184512 (2016).

[11] T. A. Bither, C. T. Prewitt, J. L. Gilison, P. E. Bierstedt, R. B. Flippen, and H. S. Young, New transition metal dichalcogenides formed at high pressure, Solid State Commun. **4**, 533 (1966).

[12] R. A. Munson, The synthesis of copper disulfide, Inorg. Chem. **5**, 1296 (1966).

[13] T. A. Bither, R. J. Bouchard, W. H. Cloud, P. C. Donohue, and W. J. Siemons, Transition metal pyrite dichalcogenides: High-pressure synthesis and correlation of properties, Inorg. Chem. **7**, 2208 (1968).

[14] H. Ueda, M. Nohara, K. Kitazawa, H. Takagi, A. Fujimori, T. Mizokawa, and T. Yagi, Copper pyrites CuS_2 and $CuSe_2$ as anion conductors, Phys. Rev. B **65**, 155104 (2002).

[15] R. A. Munson, W. DeSorbo, and J. S. Kouvel, Electrical, magnetic, and superconducting properties of copper disulfide, J. Chem. Phys. **47**, 1769 (1967).

[16] G. Krill, P. Panissod, M. F. Lapierre, F. Gautier, C. Robert, and M. N. Eddine, Magnetic properties and phase transitions of the metallic CuX_2 dichalcogenides (X = S, Se, Te) with pyrite structure, J. Phys. C **9**, 1521 (1976).

[17] F. Gautier, G. Krill, P. Panissod, and C. Robert, Magnetic-properties of CuS_2, J. Phys. C **7**, L170 (1974).

[18] M. Kakihana, T. D. Matsuda, R. Higashinaka, Y. Aoki, A. Nakamura, D. Aoki, H. Harima, M. Hedo, T. Nakama, and Y. Ōnuki, Superconducting and Fermi surface properties of pyrite-type compounds CuS_2 and $CuSe_2$, J. Phys. Soc. Jpn. **88**, 014702 (2019).

[19] M. Kontani, T. Tutui, T. Moriwaka, and T. Mizukoshi, Specific heat and NMR studies on the pyrite-type superconductors CuS_2 and $CuSe_2$, Physica B **284**, 675 (2000).

[20] G. Vanderschaeve and B. Escaig, Electron microscopy study of transition metals disulfides with pyrite structure, Mater. Res. Bull. **11**, 483 (1976).

[21] Y. X. Yin, J. Coulter, J. Christopher, and N. Prineha, Theoretical investigation of charge density wave instability in CuS_2, Phys. Rev. Mater. **4**, 104001 (2020).

[22] See Supplemental Material at http://link.aps.org/supplemental/10.1103/PhysRevMaterials.6.014802 for details about the temperature-dependent specific heat $C(T)$, electron diffraction patterns, and the temperature dependences of resistivity $\rho(T)$ at 1.8 and 2.3 GPa under various magnetic fields.

[23] J. A. Wilson, F. J. Di Salvo, and S. Mahajan, Charge-Density Waves in Metallic, Layered, Transition-Metal Dichalcogenides, Phys. Rev. Lett. **32**, 882 (1974).

[24] E. H. Brandt, Properties of the ideal Ginzburg-Landau vortex lattice, Phys. Rev. B **68**, 054506 (2003).

[25] E. H. Brandt, Some properties of the ideal Ginzburg-Landau vortex lattice, Physica C **404**, 74 (2004).

[26] Y. Takano, N. Uchiyamab, S. Ogawab, N. Mori, Y. Kimishimad, S. Arisawaa, A. Ishii, T. Hatano, and K. Toganoa, Superconducting properties of $Cu\,S_{2-x}Se_x$ under high pressure, Physica C **341–348**, 739 (2000).

[27] Q. Dong, Q. J. Li, S. J. Li, S. H. Shi, S. F. Niu, S. J. Liu, R. Liu, B. Liu, X. Luo, J. G. Si, W. J. Lu, N. Hao, Y. P. Sun, and B. B. Liu, Structural phase transition and superconductivity hierarchy in $1T$-TaS_2 under pressure up to 100 GPa, npj Quantum Mater. **6**, 20 (2021).

[28] S. X. Xu, Z. Y. Liu, P. T. Yang, K. Y. Chen, J. P. Sun, J. H. Dai, Y. Y. Yin, F. Hong, X. H. Yu, M. Q. Xue, J. Gouchi, Y. Uwatoko, B. S. Wang, and J. G. Cheng, Superconducting phase diagrams of S-doped $2H$-$TaSe_2$ under hydrostatic pressure, Phys. Rev. B **102**, 184511 (2020).

[29] W. Wang, B. S. Wang, Z. B. Gao, G. Tang, W. Lei, X. J. Zheng, H. Li, X. Ming, and C. Autieri, Charge density wave instability and pressure-induced superconductivity in bulk $1T$-NbS_2, Phys. Rev. B **102**, 155115 (2020).

[30] Q. Y. Zhang, L. Y. Gan, Y. C. Cheng, and S. Udo, Spin polarization driven by a charge-density wave in monolayer $1T$-TaS_2, Phys. Rev. B **90**, 081103(R) (2014).

[31] S. Berri and N. Bouarissa, Electronic structure and fundamental properties of MoX_2 (X = Te, Se and S) compound materials at high pressures and elevated temperatures, Computat. Condens. Matter **28**, e00574 (2021).

[32] K. Mahalakshmi, S. Sambasivam, and V. S. Sathyakumari, Electronic, thermal and superconducting properties of metallic CuS_2 compound with pyrite structure: An *ab initio* study, High Temp.-High Press. **44**, 25 (2015).